Available online at www.sciencedirect.com
SCIENCE DIRECT®
Journal of Power Sources 130 (2004) 254–259
JOURNAL OF POWER SOURCES
www.elsevier.com/locate/jpowsour

Lithium insertion into manganese dioxide electrode in MnO_2/Zn aqueous battery Part I. A preliminary study

Minakshi Manickam [a,*], Pritam Singh [a], Touma B. Issa [a], Stephen Thurgate [a], Roland De Marco [b]

[a] *Division of Science and Engineering, Murdoch University, Murdoch 6150, WA, Australia*
[b] *Department of Applied Chemistry, Curtin University of Technology, Kent Street, Bentley 6102, WA, Australia*

Received 12 November 2003; accepted 10 December 2003

Abstract

The discharge characteristics of manganese dioxide (γ-MnO_2 of electrolytic manganese dioxide (EMD) type) as a cathode material in a Zn–MnO_2 battery containing saturated aqueous LiOH electrolyte have been investigated. The X-ray diffraction (XRD) and X-ray photoelectron spectroscopy (XPS) data on the discharged material indicate that lithium is intercalated into the host structure of EMD without the destruction of its core structure. The XPS data show that a layer of insoluble material, possibly Li_2CO_3, is deposited on the cathode, creating a barrier to H_2O, thus preventing the formation of Mn hydroxides, but allowing the migration of Li ions into the MnO_2 structure. The cell could be reversibly charged with 83% of voltaic efficiency at 0.5 mA/cm^2 current density to a 1.9 V cutoff voltage. The percentage utilization of the cathode material during discharge was 56%.

Keywords: Aqueous battery; Lithium insertion; MnO_2; Electrolyte; XRD; XPS

1. Introduction

Materials with the general formula $LiMO_2$ (M = Mn, Fe, Ni, Co) [1–4] have received a great deal of attention recently as prospective cathode materials for use in a non-aqueous cell. Of the four transition metals above, Mn and Fe are by far the most attractive with regard to toxicity concerns and from an economic point of view. Manganese has an added advantage in that it can support higher oxidation states, which makes it suitable as a cathode material. Manganese dioxide is also used as the positive active (cathode) material in Leclanche and alkaline manganese batteries [5], which together dominate the primary battery market. Electrolytic manganese dioxide (EMD) is one of the most important materials for both aqueous and non-aqueous cells. Extensive research [6] has been done on lithium insertion into γ-MnO_2 of EMD type in non-aqueous cells. Intercalation of Li^+ ions into host γ-MnO_2 structures is widely reported [6,7] in non-aqueous batteries. There is very limited information on intercalation occurring in aqueous media [8]. If this mechanism is possible in aqueous media the MnO_2 cathode could become rechargeable similar to non-aqueous Li–MnO_2 batteries. Hence, it could open up a new field of rechargeable alkaline batteries that utilize MnO_2 as the cathode active material. With this in mind, we have investigated the use of lithium hydroxide (LiOH) in place of traditional potassium hydroxide as the battery electrolyte in alkaline Zn–MnO_2 batteries. The main objective of this work is to investigate whether intercalation of Li^+ into the host structure of MnO_2 does occur. Other objectives of this work are:

- the effect of LiOH on MnO_2 utilization and voltaic efficiency;
- the electrochemical characteristics and the discharge mechanism of MnO_2 as a cathode material.

2. Short review of γ-MnO_2 as a cathode material

Synthetic manganese dioxides and particularly those made by electrodeposition (EMD) are used in high performance batteries. EMD is a member of the imperfectly crystalline γ-manganese dioxides [9], which are related to ramsdellite and pyrolusite by various proportions of the

* Corresponding author. Tel.: +61-8-9360-2719; fax: +61-8-9310-1711.
E-mail address: minakshi@central.murdoch.edu.au (M. Manickam).

0378-7753/$ – see front matter © 2003 Elsevier B.V. All rights reserved.
doi:10.1016/j.jpowsour.2003.12.018

types of random structural disorder [10], de Wolff disorder and microtwinning. γ-MnO_2 shows a high complexity in its chemical composition as well as in its crystallographic structure. Among the different models proposed to account for the γ-MnO_2 for a practical battery system [11], Ruetschi's model [12] presents a quantitative report in the cation vacancy in MnO_2. In the Ruetschi's lattice-vacancy model of γ-MnO_2, it is considered that

1. Each manganese ion in the MnO_2 structure is octahedrically co-coordinated to six nearest oxygen ions, and each oxygen ion is co-coordinated to three nearest manganese ions. The MnO_6 octahedral are arranged in the crystal as to share edges and corners. Since the ionic radii of O^{2-} ions (1.40 Å) are much larger than Mn^{4+} ions (0.53 Å) the lattice resembles a dense packing of O^{2-} ions, with the small Mn^{4+} ions orderly arranged in the edge shared MnO_6 octahedral chains between O^{2-} layers [13]. This is the usual crystallographic description.
2. In this structure, a fraction of Mn^{4+} ions are missing in the Mn^{4+} sub-lattice. Each empty Mn^{4+} site is, for charge compensation, coordinated to four protons, the latter being present in the form of four OH^- ions. The OH^- ions replace O^{2-} in the lattice without significant volume change of the unit cell, the ionic radii of O^{2-} and OH^- being very similar [14]. Normal unit cell parameters are thus maintained.
3. A fraction of the Mn^{4+} ions are replaced by Mn^{3+}. For each Mn^{3+} present, one proton is introduced for charge compensation. These protons for further OH^- ions, replacing O^{2-} in the lattice.
4. Thus the lattice is composed of O^{2-}, OH^-, Mn^{4+} and Mn^{3+} ions and Mn vacancies. All the structural water is present in the form of OH^- ions, associated with either Mn vacancies, or Mn^{3+} ions.

The γ-MnO_2 can be described by the chemical formula $Mn^{4+}_{(1-Y-Z)}Mn^{3+}_{(Z)}O^{2-}_{(2-4Y-Z)}OH^{-}_{(4Y-Z)}$, where Y is the cation vacancy fraction and Z the fraction of Mn^{3+} ions replacing Mn^{4+} in the manganese sub-lattice.

The electrochemical reactions that take place at the manganese dioxide electrode in aqueous cell [15] during the discharge process of a battery corresponding to the insertion of X can then be described by the following equations:

For $0 < X < 1 - Y - Z$

$$Mn^{4+}_{(1-Y-Z)}Mn^{3+}_{(Z)}O^{2-}_{(2-4Y-Z)}(OH^-)_{(4Y+Z)} + xH^+ + xe^- \rightarrow Mn^{4+}_{(1-Y-Z-X)}Mn^{3+}_{(Z+X)}O^{2-}_{(2-4Y-Z-X)}(OH^-)_{(4Y+Z+X)} \quad (1)$$

where e^- represents an electron. Eq. (1) is generally reported in the literature [15] in the following simplified way:

$$\gamma\text{-}MnO_2 + xH^+ + xe^- \rightarrow MnO_{2-x}(OH)_x \quad (2)$$

For $X > 1 - Y - Z$

$$Mn_{(1-Y)}O_{(1-3Y)}OH_{(1+3Y)} + xH^+ + xe^- \rightarrow \text{mixture of } [(Mn_2O_3 \text{ or } Mn_3O_4) + Mn(OH)_2] \quad (3)$$

The products of the materials produced after discharge in Eq. (3) is known to be electrochemically inactive, so this held as primary aqueous batteries.

In the non-aqueous lithium cells during discharge, lithium ions are inserted into the vacant sites while the Mn^{4+} ions are replaced by Mn^{3+} ions, which explains the electrochemical behavior of γ-MnO_2 associated with the discharge of Li–MnO_2 batteries [7]. The electrochemical reactions for non-aqueous lithium cells have been generally written as

$$MnO_2 + Li^+ + e^- \underset{\text{charge}}{\overset{\text{discharge}}{\rightleftarrows}} LiMnO_2 \quad (4)$$

3. Experimental

The γ-MnO_2 of EMD type used in this work was purchased from the Foote mineral company. The X-ray diffraction pattern of the raw material indicated that it consisted of poorly crystallized γ-MnO_2. The theoretical maximum electrochemical capacity deliverable per unit weight for a one-electron process is 289 mAh/g.

The materials employed during electrode preparation were Zn metal for the anode and γ-MnO_2 for the cathode. The MnO_2 active material was first mixed with 20 wt.% of carbon black and with 10 wt.% of PVDF as a binder and then pressed into a disk shape with a diameter of 12 mm. Each disk was 0.5 mm thick and weighed approximately 35 mg. An electrochemical test cell was constructed with the disk as the cathode, Zn metal as the anode and filter paper as the separator. The mass of zinc was at least 10-fold in excess of that required for the stoichiometric reaction between Zn and MnO_2. The electrolyte was a saturated solution of lithium hydroxide (LiOH) containing 1 mol l^{-1} zinc sulfate ($ZnSO_4$). Analytical reagent grade of zinc sulphate heptahydrate ($ZnSO_4{\cdot}7H_2O$; Ajax Chemicals), lithium hydroxide monohydrate ($LiOH{\cdot}H_2O$; Sigma Chemicals company) and potassium hydroxide (KOH; Ajax Chemicals) were dissolved in deionized water to prepare solutions of required concentrations.

The cells were charged/discharged galvanostatically at 0.5 mA/cm^2 by using an EG&G Princeton Applied Research Potentiostat/Galvanostat model 273A, operated by model 270 software (EG&G). The cutoff discharge and charge voltages were 1.0 and 1.9 V, respectively. All electrochemical measurements were carried out at ambient room atmosphere (25 ± 1 °C).

The products formed during charge and discharge cycles were characterized by a Siemens X-ray diffractometer using Philips Co Kα radiation. X-ray photoelectron spectroscopy (Kratos Ultra Axis Spectrometer) using monochromatic Al Kα (1486.6 eV) radiation was used to analyze the chemical

binding energy of the samples. The XPS analysis was started when the pressure in the analysis chamber fell below 1×10^{-9} h Pa.

4. Results and discussion

4.1. Performance characteristics of Zn–MnO_2-aqueous LiOH cell

There is substantial literature on the performance characteristics of MnO_2 in alkaline aqueous Zn–MnO_2 cells using potassium hydroxide (KOH) as the electrolyte. The use of highly conductive potassium hydroxide as the electrolyte, results in a lower internal resistance [16]. However, the conductivity of the electrolyte is changed by the dissolution of $Zn(OH)_2$ from the anode during the discharge cycle. Kordesch et al. [17] has reported that the discharge behavior of the cathode material, MnO_2, in the alkaline KOH electrolyte occurs in an heterogeneous phase reaction, i.e. MnO_2 being converted to Mn_2O_3. Hence, the MnO_2 lattice expands and, at a certain point of discharge, the mechanism changes to an irreversible portion of the MnO_2 reduction process. To understand the effect of replacing KOH with LiOH in Zn–MnO_2 cell, we have carried out discharge cycles on two identical cells, both containing 1 M $ZnSO_4$, but one containing saturated KOH and the other LiOH aqueous solution. The results for the first discharge cycle for both the cells are shown in Fig. 1. It can be seen that the discharge curve for the cell with KOH is quite different from that of the LiOH cell (Fig. 1(a) and (b)). The cathode utilization for the KOH cell was 41% (120 mAh/g) as compared to 56% (162 mAh/g) for the LiOH cell using a 1 V cutoff for both cells. The discharge capacity for LiOH, Fig. 1(b), was higher and the decrease in cell potential was lower when LiOH was the electrolyte. For the KOH, the potential underwent a sharp fall at 1.0 V.

The reversibility of the cell Zn–MnO_2 using saturated aqueous LiOH containing 1 mol l^{-1} of $ZnSO_4$ as the electrolyte was investigated and the results are shown in Fig. 2. The cell could be reversibly discharged and charged. As can be seen in Fig. 2, the shape of the discharge curve is characterized by a sharp drop in voltage to 1.3 V, and a gradual downward-sloping potential profile until the 1 V cutoff voltage is reached. The cathode material utilization was calculated from the initial weight of the active MnO_2 in the cathode and the voltaic efficiency from the observed average charge/discharge voltages. The material utilization of 56% (162 mAh/g) and the voltaic efficiency of 83% were obtained. During the charge/discharge cycle, the cell potential changed continuously, indicating a homogenous phase reaction.

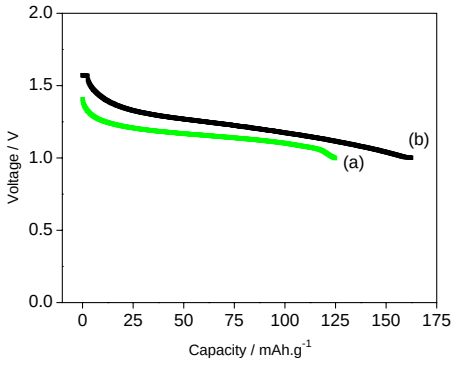

Fig. 1. First discharge curve of Zn–MnO_2 cells using saturated aqueous of (a) KOH and (b) LiOH containing 1 mol l^{-1} of $ZnSO_4$ under identical conditions.

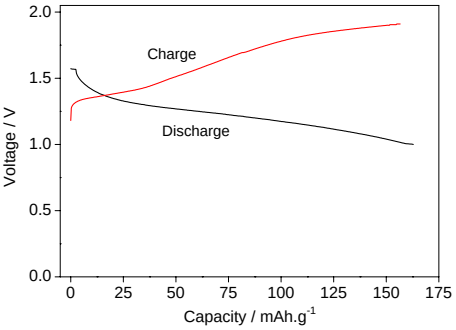

Fig. 2. The first discharge–charge profile of Zn–MnO_2 cells using saturated aqueous LiOH containing 1 mol l^{-1} of $ZnSO_4$ as the electrolyte.

4.2. Characterization of the cathode material

In order to determine the mechanism by which the cathode material γ-MnO_2 discharges in Zn–MnO_2 cell in LiOH electrolyte, characterization of the discharged cathode material produced was investigated by XRD and XPS. Fig. 3(a) and (b) shows the X-ray diffraction patterns of the cathode material γ-MnO_2 before and after discharge. Due to the poor crystallinity of the cathode material, the X-ray diffraction pattern in Fig. 3(a) shows a few broad Bragg reflections. As can be seen in Fig. 3(b), an evolution of a new sharp peak at a *d*-spacing of 3.27 Å, and the corresponding shoulder at a *d*-spacing of 3.18 Å is observed in the discharged γ-MnO_2 material. Clearly, these peaks do not correspond to any of

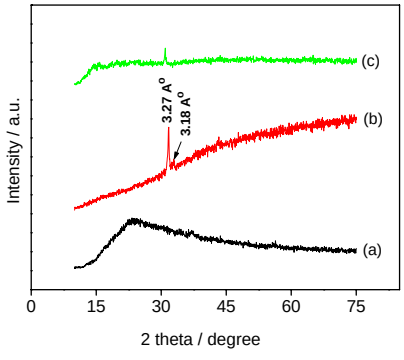

Fig. 3. X-ray diffraction patterns changes of γ-MnO_2 after the electrochemical cycling in an aqueous battery: (a) γ-MnO_2 (before discharge); (b) upon discharge; (c) upon subsequent charge.

the MnOOH structure, Mn_2O_3 or Mn_3O_4 which are reported to be formed when aqueous KOH based Zn/MnO_2 cells are discharged. This suggests that the discharge mechanism of this cathode material is not the same as that commonly reported for alkaline Zn–MnO_2 batteries. A close examination of our data suggests that the peaks correspond to those reported for non-aqueous lithium cells by Aurbach and coworkers [18]. The peaks corresponding to the *d*-spacing of 3.27 and 3.18 Å can be assigned to lithium intercalated γ-β-MnO_2 (a hexagonal close-packed arrangement of oxygen, in which Mn and Li ions are located at octahedral sites), and the co-existence of two phases. The MnO_6—octahedral structure includes tunnels (1 × 1) and (1 × 2) in which Li ions should intercalate/de-intercalate during discharge/charge process. Moreover, a comprehensive study of the intercalation mechanism by Ohzuku et al. [19] showed a similar diffraction peak at a *d*-spacing of 3.27 Å for their heat-treated γ-MnO_2 during the discharge in a non-aqueous lithium cell, and ascribed it to γ-β-MnO_2. Fig. 3(c) also shows the X-ray diffraction pattern of the cathode material after recharging the discharged battery. A decrease in the intensity of the peak corresponding to the γ-β-MnO_2 occurs. Hence, we can infer that the lithium intercalation is electrochemically reversible. However, it should be noted that the peak shifts to a lower angle. This is to be expected as the lithium ion is de-intercalated from the structure [20].

The cathode material formed during the discharge cycle was further characterized by X-ray photoelectron spectroscopy (XPS), a powerful tool for surface studies. A wide scan XPS spectrum of the surface (0–1400 eV) of this material is shown in Fig. 4. The important feature to notice in Fig. 4 is the highly dominant O 1s peak, while the signals of other elements of interest are quite weak. The surface of the cathode material was covered with a thick overlayer of material deposited during the discharge of the battery. This outer layer contained the elements C, O, and Li. H cannot be detected with XPS. Consideration of the binding energies and relative concentrations suggests that this overlayer was composed of a mixture of LiOH and Li_2CO_3. This outer

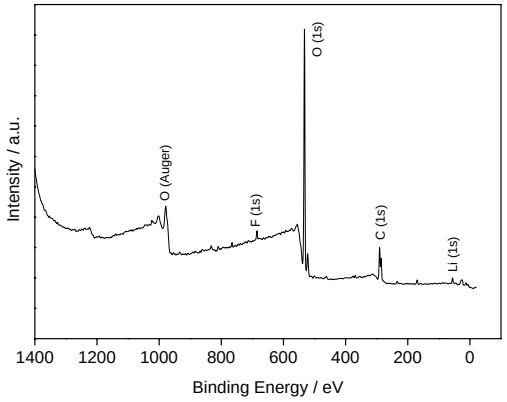

Fig. 4. XPS spectra (wide scan) of the cathode manganese dioxide (γ-MnO_2) after electrochemical lithium intercalation.

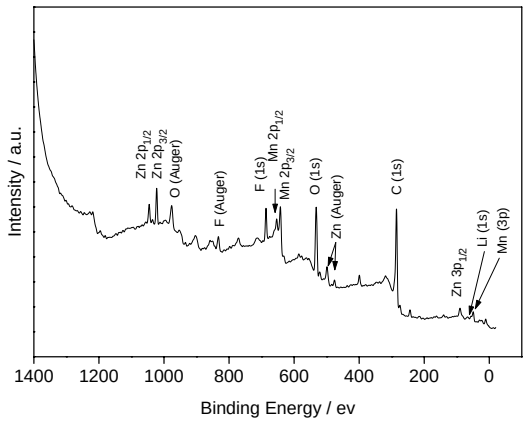

Fig. 5. XPS spectra (wide scan) of the cathode manganese dioxide (γ-MnO_2) after electrochemical lithium intercalation upon argon ion etching for 5 h.

layer required 5 h of ion bombardment (4.0 kV, 2 μA, 500 μ spot) to remove it and reveal the underlining material. We estimate the thickness of this material as 0.5 μm (assuming an etch rate of 1.7 nm/min). The XPS spectrum of the material after prolonged etching for 5 h (shown full scale, Fig. 5) reveals the presence of the underlying elements Zn, Mn, and Li, with a much reduced intensity of O 1s. It is interesting to note that Zn was not seen on the undisturbed outer surface, but is present in the active surface of the MnO_2 material. This is the clear evidence that the overlayer is porous with ions. These can travel through the overlayer to the active MnO_2 material underneath. Li_2CO_3 is insoluble. Fig. 6 shows the variation in concentration of the Li_2CO_3 and LiOH with depth. It is clear that the insoluble Li_2CO_3 forms a barrier to H_2O, but that the LiOH is able to move through the structure. The concentration of LiOH falls with depth into the solid in a profile that is not inconsistent with a diffusion driven process.

In order to view the spectra associated with each of the elements presented in Fig. 5, the XPS spectra over regions specific to elements of interest were recorded over five sweeps. Figs. 7–10 show the high resolution XPS spectra, as a function of argon ion etching of the material. It can be seen

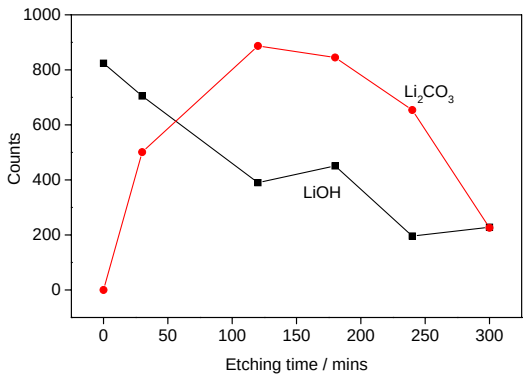

Fig. 6. Variation in concentration of the Li_2CO_3 and LiOH upon depth profiling.

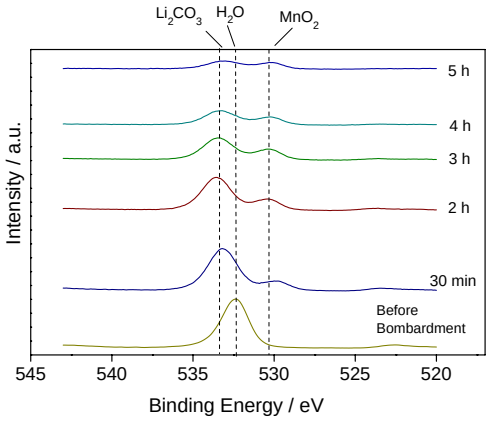

Fig. 7. XPS spectra of O 1s for the cathode manganese dioxide (γ-MnO_2) after electrochemical lithium intercalation, time in figure indicates the etching duration.

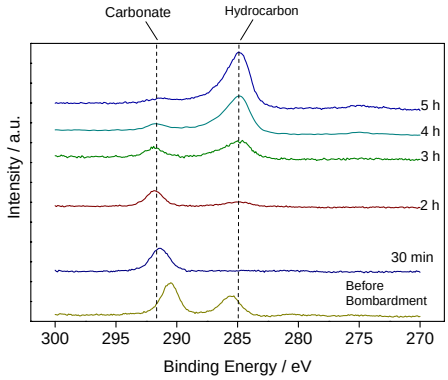

Fig. 8. XPS spectra of C 1s for the cathode manganese dioxide (γ-MnO_2) after electrochemical lithium intercalation, time in figure indicates the etching duration.

in Fig. 7 that, after the first 30 min of bombardment, the O 1s peak at 532 eV disappears. Instead two new peaks emerged one at 533 and the other at 530.1 eV. Furthermore, the peak intensity of the signal at 533 eV decreased with increased argon ion etching period, whereas the intensity of second signal peak at 530.1 eV remained fairly constant. Based upon binding energies as reported in the literature [21], we assign the peak at 533 eV to Li_2CO_3, which is expected to result from the exposure of LiOH to air and the second peak at 530.1 eV to MnO_2, present in the material itself.

Fig. 8 shows the XPS spectra of C 1s for the cathode material (γ-MnO_2) after discharge. Two types of carbon peaks were observed, one at 285 eV that we assign to the hydrocarbons present in the electrode material, and the other at 291 eV can be assigned to carbon associated with Li_2CO_3. The intensity of the peak at 285.0 eV, which had a very weak signal before argon ion bombardment, increased in intensity on continuous etching of the overlayer. The other peak at 291 eV in Fig. 7 corresponding to Li_2CO_3 is formed and then removed upon etching indicating that insoluble Li_2CO_3 forms a barrier to H_2O. This is consistent with the change in the O 1s as discussed above for Fig. 7.

Fig. 9 focuses on the region where Li 1s and Mn 3s are expected to occur. It can be seen that the peak at 55.6 eV, which was assigned to the presence of Li_2CO_3 in the unetched material, decreased in intensity on etching. The prolonged etching showed the emergence of another peak at 56.3 eV. This peak is assigned to the underlying lithium intercalated within manganese dioxide, Li_xMnO_2. The basis of this assignment is that the Li species is such that the binding energy of the 1s electron is greater than that of Li in Li_2CO_3. This is likely to be the case with the Li^+ ion intercalated into the highly oxidizing environment of the MnO_2 structure. The signal at 48 eV, which was barely visible in the unetched material, increased in intensity as the etching period increased. This signal is quite pronounced after 3 h of etching and clearly indicates the presence of Mn, as seen in Fig. 9.

Fig. 10 shows the XPS spectra of Mn 2p. As was observed for the Mn 3s signal, prolonged argon gas etching (3 h) also resulted in increased intensity of the Mn $2p_{1/2}$ and $_{3/2}$ spin orbit split components. Thus, removal of the outer layer by argon ion etching assists in exposing the true discharge products of the cathode material in saturated LiOH

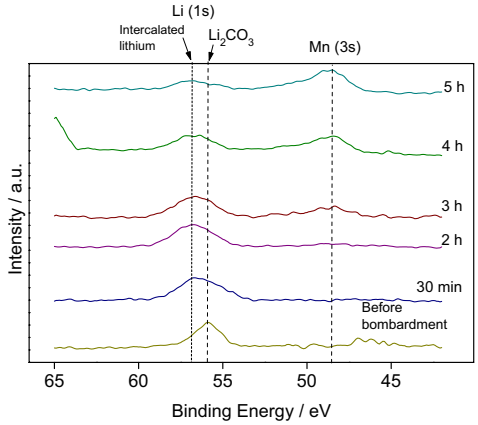

Fig. 9. XPS spectra of Li 1s and Mn 3s for the cathode manganese dioxide (γ-MnO_2) after electrochemical lithium intercalation, time in figure indicates the etching duration.

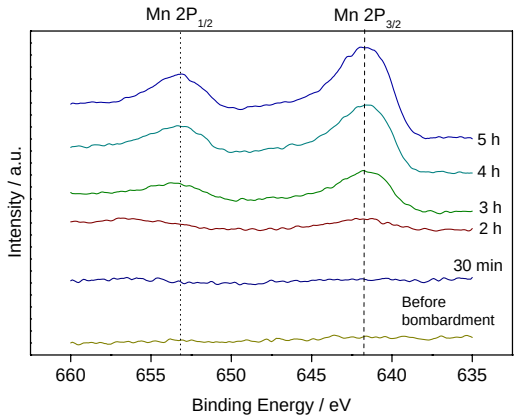

Fig. 10. XPS spectra of Mn 2p for the cathode manganese dioxide (γ-MnO_2) after electrochemical lithium intercalation, time in figure indicates the etching duration.

electrolyte. From the evidence based on the XRD and XPS studies, it can be concluded that lithium is indeed intercalated electrochemically into the host framework of γ-MnO_2 when aqueous LiOH is the electrolyte.

5. Conclusion

The charge–discharge cycle behavior of a novel Zn–MnO_2 alkaline battery containing aqueous LiOH electrolyte has been investigated. It is found that the battery with aqueous LiOH electrolyte functions quite differently from the traditional battery, which uses aqueous KOH. When the battery is discharged in cells containing aqueous LiOH, lithium is intercalated into the host framework structure of the positive electrode material, manganese dioxide (γ-MnO_2). The formation of this material is confirmed through XRD and XPS studies of the positive electrode material (γ-MnO_2) before and after discharge and upon subsequent charge/discharge cycling. The mechanism of discharge of γ-MnO_2 differs from the usual products MnOOH, Mn_2O_3 or Mn_3O_4, which are formed when KOH is the electrolyte. The LiOH based battery can be reversibly charged. Under the investigated conditions, 56% (162 mAh/g) of the theoretical capacity of the positive electrode active material (γ-MnO_2) to 1 V cutoff voltage could be achieved. The voltaic efficiency is found to be 83% when the battery is charged and discharged at 0.5 mA/cm^2 of current density.

Acknowledgements

One of us (M. Minakshi) is particularly grateful to Murdoch University for a research scholarship.

References

[1] M. Manickam, K. Minato, M. Takata, J. Electrochem. Soc. 150 (2003) 1085, and references therein.
[2] C. Delmas, I. Saadoune, Solid State Ionics 53–56 (1992) 370.
[3] J.N. Reimers, J.R. Dahn, J. Electrochem. Soc. 139 (1992) 2091.
[4] E. Rossen, J.N. Reimers, J.R. Dahn, Solid State Ionics 62 (1993) 53.
[5] F.L. Tye, in: M. Barak (Ed.), Electrochemical Power Sources, Peter Peregrinus, London, 1980, p. 50.
[6] H. Ikeda, J. Power Sour. 9 (1983) 329.
[7] G. Pistoia, J. Electrochem. Soc. 129 (1982) 1861.
[8] R.L. Deutscher, T.M. Florence, R. Woods, J. Power Sour. 55 (1995) 41.
[9] C. Mondolini, M. Laborde, J. Rioux, E. Andoni, C. Levy-clement, J. Electrochem. Soc. 139 (1992) 954.
[10] Y. Chabre, J. Pannetier, Prog. Solid State Chem. 23 (1995) 1.
[11] A. Kozawa, R.A. Powers, J. Electrochem. Soc. 113 (1966) 870; A. Kozawa, R.A. Powers, J. Electrochem. Soc. 115 (1968) 122.
[12] P. Ruetschi, R. Giovanoli, J. Electrochem. Soc. 135 (1988) 2663.
[13] R. Giovanoli, in: Proceedings of the Manganese Dioxide Symposium, vol. 2, Tokyo, 1980; B. Schumm, H.M. Joseph, A. Kozawa (Eds.), Paper 7, I.C. Sample office, Cleveland, OH, p. 113.
[14] R.D. Shannon, Acta Crystallogr. Sect. A 32 (1976) 751.
[15] C. Mondoloni, M. Laborde, J. Rioux, E. Andoni, C. Levy-clement, J. Electrochem. Soc. 139 (1992) 954.
[16] D. Linden (Ed.), Handbook of Batteries and Fuel Cells, McGraw-Hill, New York, NY, 1984.
[17] K. Kordesch, J. Gsellmann, M. Peri, K. Tomantschger, R. Chemelli, Electrochim. Acta 26 (1981) 1495.
[18] E. Levi, E. Zingrad, H. Teller, M.D. Levi, D. Aurbach, E. Mengeritsky, E. Elster, P. Dan, E. Granot, H. Yamin, J. Electrochem. Soc. 144 (1997) 4133.
[19] T. Ohzuku, M. Kitagawa, T. Hirai, J. Electrochem. Soc. 136 (1989) 3169.
[20] M. Manickam, J. Power Sour. 113 (2003) 179.
[21] Perkin Elmer Corporation, Handbook of X-ray Photoelectron Spectroscopy, Physical Electronics Division, Perkin Elmer Corporation, USA, October 1992.